

**BIMODAL POROUS CERAMIC MEMBRANE VIA NANOSIZED  
POLYSTYRENE TEMPLATING: SYNTHESIS, CHARACTERIZATION  
AND PERFORMANCE EVALUATION**

**by**

**LEO CHOE PENG**

**Thesis submitted in fulfillment of the requirements  
for the degree of  
Doctor of Philosophy**

**May 2008**

## ACKNOWLEDGEMENTS

On top of the list of acknowledgements, I would like to thank my parents Mr. Leo Kim Bin and Madam Yeoh Sok Kim for giving never-ending love and support in my life and, of course, my study. I'm grateful that I have a big family (including Chee Hooi, Chin Tai, Choe Yin, You Foo, Choe Qun, Choe Shuang, Marcus and Amanda) to share the sweet and sour in these years.

Apart from my family, two people have been extremely important in my scientific development: Prof. Abdul Latif Ahmad and Dr. Syamsul Rizal Abd. Shukor who made it possible for me to start my research in USM. Your practical view and guidance on my study was of the utmost importance. Thank you for the endless support throughout these three years. In addition, I would like to express my grateful thanks to USM for providing PASCA scholarship and USM Short Term Grant.

Also, thanks to friends in USM for their company and guidance, Ooi, Sumathi, Derek, Siew Chun, Ramesh, Choi Yee, Pei Chin, Siang Piao, Sim, and Sunarti. Without you all, labs and Ph. D. room are peaceful but dull. Special thanks to Choo Weng, Ee Mee and Prof. Wahab too for encouraging me to continue study. Not forgetting also, many thanks to the staff of School of Chemical Engineering especially lecturers, office staff and technicians. It is a pity that it is not possible here to thank everybody in and around USM that I got to know personally through these years. Still, to everyone who is listed and all others that I forgot, I will miss you very much.

## TABLE OF CONTENTS

<b>Acknowledgement</b>	ii
<b>Table of Contents</b>	iii
<b>List of Tables</b>	ix
<b>List of Figures</b>	xiii
<b>List of Plates</b>	xviii
<b>List of Symbols</b>	xix
<b>List of Abbreviations</b>	xxv
<b>Abstrak.</b>	xxiv
<b>Abstract</b>	xxvi

### CHAPTER 1 - INTRODUCTION

1.1	Membrane Separation Technology	1
1.1.1	Nanofiltration (NF)	3
1.1.2	Ceramic membranes with high stability	4
1.1.3	Sol-gel method for the preparation of ceramic membranes	6
1.1.4	General application of ceramic membranes in liquid phase separation	9
1.2	Problem Statements	11
1.3	Research Objectives	14
1.4	Research Scope	15
1.5	Organization of the Thesis	17

### CHAPTER 2 - LITERATURE REVIEW

2.1	Membrane Support for Sol-gel Derived Membranes	21
2.1.1	Common preparation methods of membrane supports	21
2.1.2	Tape casting of asymmetric membrane supports	23
2.2	Tailoring Pores in Ceramics by Templating	27
2.2.1	Sphere templating for sol-gel derived ceramics	31
2.2.2	Sphere templates and its removal methods	34

2.2.3	Ordering of spheres and interstices filling with sols	37
2.2.4	Ceramics templated by spheres and related applications	40
2.3	Sol-gel Derived Ceramic Membranes for Nanofiltration (NF)	43
2.3.1	Sol-gel derived ceramic membranes	44
2.3.2	Ceramic membranes for nanofiltration (NF)	51
	2.3.2(a) Separation of neutral solutes	52
	2.3.2(b) Separation of charged solutes	53
	2.3.2(c) Organic molecules and electrolyte separation	58

### **CHAPTER 3 - NANOFILTRATION TRANSPORT MODEL**

3.1	Transport in Membranes	62
3.2	Transport equation: Extended Nernst-Planck (ENP)	63
3.3	Donnan Steric Pore Model (DSPM) for Ion Transport through NF Membranes	65
3.3.1	Model assumptions	65
3.3.2	Basic equation of Donnan Steric Pore Model (DSPM)	66
3.3.3	Equilibrium partitioning	69
3.3.4	Concentration polarization	70
3.3.5	Pore size and effective thickness/porosity determination	71
3.3.6	Effective volume charge density determination	72
3.4	Combined Film Theory-extended Nernst-Planck Equation (CF-ENP)	74

### **CHAPTER 4 - MATERIALS AND METHODS**

4.1	Materials and Chemicals	78
4.2	Membrane Support Preparation Method	81
4.2.1	Preparation of alumina slurry	81

4.2.2	Doctor blade casting of alumina green tapes	81
4.2.3	Design of experiments (DOE) for studying effect of organic mixture added and casting gap on tape thickness	82
4.2.4	Pressing and sintering of $\alpha$ -alumina membrane support	84
4.2.5	Filtration unit and experimental rig for liquid permeation test	85
4.2.6	Water permeability test	86
4.2.7	Design of experiments (DOE) for preliminary study on the significance of tape thickness and organic content on support permeability flux	87
4.2.8	Design of experiments (DOE) for preparing membrane support with high permeability and acceptable yield loss	88
4.2.9	Characterization of support structure using scanning electron microscope (SEM)	90
4.3	Synthesis and Characterization of Template and Bimodal Porous $\gamma$ -Alumina	90
4.3.1	Synthesis of nanosized polystyrene (PS) spheres	90
4.3.2	Characterization of template using transmission electron microscope (TEM)	91
4.3.3	Preparation of boehmite sol	91
4.3.4	Preparation of $\gamma$ -alumina with bimodal pore size distribution	92
4.3.5	Thermal gravimetric analysis (TGA) of boehmite sols with different quantities of templating units	93
4.3.6	Viscosity measurement for boehmite sols with different quantities of templating units	93
4.3.7	Characterization of $\gamma$ -alumina using transmission electron microscope (TEM)	93
4.3.8	Characterization of $\gamma$ -alumina using Fourier- transform infrared (FT-IR)	94
4.3.9	Characterization of $\gamma$ -alumina using X-ray diffraction (XRD)	94
4.3.10	Study on the effect of heat treatment on templated pores	94
4.3.11	N <sub>2</sub> adsorption/desorption	94
4.3.12	Determination of adsorption rate constant for $\gamma$ -alumina with different porous structures	95

4.4	Synthesis and Characterization of Bi-layered Membranes with Bimodal Porous Intermediate Layers	97
4.4.1	Synthesis of $\gamma$ -alumina thin layers with bimodal pore size distribution	97
4.4.2	Characterization of supported $\gamma$ -alumina layers using scanning electron microscope (SEM)	97
4.4.3	Determination of permeability and specific resistance for supported $\gamma$ -alumina layers	97
4.4.4	Polyethylene glycol (PEG) retention test for pore size determination of $\gamma$ -alumina thin layers	99
4.4.5	Determination of the ratio of effective membrane thickness to porosity for $\gamma$ -alumina layers	99
4.4.6	Synthesis of surfactant templated silica and silica/ $\gamma$ -alumina bi-layered membranes	101
4.4.7	Characterization of surfactant templated silica using transmission electron microscope (TEM), X-ray diffraction (XRD) and N <sub>2</sub> adsorption/desorption	102
4.4.8	Characterization of bi-layered membranes using scanning electron microscope (SEM) and energy dispersive X-ray microanalysis (EDX)	102
4.4.9	Water permeability test for bi-layered membranes	102
4.4.10	Determination of permeability and specific resistance for silica layers	102
4.4.11	PEG retention test for pore size determination of silica layers	102
4.4.12	Determination of the ratio of effective membrane thickness to porosity for silica layer	103
4.5	Performance Evaluation of Bi-layered Membranes in Organic and Inorganic Ions Separation	103
4.5.1	Dye separation test	103
4.5.2	Measurement of dye content	104
4.5.3	Study of flux decline due to osmotic pressure, concentration polarization and adsorption	104
4.5.4	Salt separation test	105
4.5.5	Measurement of pH	106
4.5.6	Measurement of NaCl Content	106
4.5.7	Determination of charge density ( $X_d$ ) for bi-layered membranes	107
4.5.8	Determination of transport mechanism of salt through bi-layered membranes	107

4.6	Performance Evaluation of Bi-layered Membranes with Bimodal Porous Intermediate Layer in Dye-Salt-Water Separation	108
4.6.1	Measurement of NaCl content in permeate samples from dye-salt-water separation	108
4.6.2	Measurement of dye content in permeate samples from dye-salt-water separation	108
4.6.3	Determination of permeate flux in permeate samples from dye-salt-water separation	109
4.6.4	Response surface method (RSM) for nanofiltration (NF) of dye-salt-water separation.	109
4.6.5	Optimization of dye-salt-water separation using nonlinear programming method	111

## **CHAPTER 5 – RESULTS AND DISCUSSION**

5.1	Preparation of $\alpha$ -Alumina Support from Green Tapes	112
5.1.1	Linear model for casting green tapes with different organic contents and thicknesses	112
5.1.2	Preliminary study on significant factors affecting support permeability	119
5.1.3	Preparation of membrane supports with high permeability and acceptable yield loss	123
5.1.4	Verification of deduced quadratic models for support permeability and yield loss	129
5.2	Bimodal Porous $\gamma$ -Alumina: Template, Sol and Calcined Oxide	131
5.2.1	Characteristics of nanosized polystyrene (PS) spheres	131
5.2.2	Effect of template amount on sol characteristics	133
5.2.3	Effect of template amount on calcined $\gamma$ -alumina characteristics	137
5.2.4	Effect of heat treatment on templated secondary pores	142
5.2.5	Optimized templated $\gamma$ -alumina – porosity and adsorption kinetic study	145
5.3	Bi-layered Membrane with Bimodal Porous Intermediate Layer: Improved Permeability	150
5.3.1	Thin layers of supported $\gamma$ -alumina with different porous structures	151
5.3.2	Characteristics of templated silica	159
5.3.3	Characteristics of bi-layered membranes with different types of intermediate layers	163

5.4	Organic and Inorganic Ions Transport Characteristics of Bi-layered Membranes with Different Secondary Pore Volumes	169
5.4.1	Effect of pressure and concentration on rejection in dye separation	170
5.4.2	Effect of pressure and concentration on permeate flux in dye separation	175
5.4.3	Effect of pressure, concentration and pH on salt retention and permeate flux in salt separation	180
5.4.4	Effect of secondary pore volumes in silica/ $\gamma$ -alumina membrane on surface charge density and transport mechanism of salt	185
5.5	Response Surface Method (RSM) for Nanofiltration (NF) of Dye and Salt Mixture in Aqueous Solution	188
5.5.1	Effect of process variables on dye rejection.	191
5.5.2	Effect of process variables on salt rejection	198
5.5.3	Effect of process variables on permeation flux	207
5.5.4	Optimization using nonlinear programming method	217
<b>CHAPTER 6 - CONCLUSIONS AND RECOMMENDATIONS</b>		
6.1	Conclusions	221
6.2	Recommendations	226
<b>BIBLIOGRAPHY</b>		227
<b>APPENDIXES</b>		
Appendix A	Calibration curves and adsorption results	258
Appendix B	Example of permeation data and its calculation of $R_{real}$ and concentration at the wall	264
Appendix C	Nonlinear regression analysis for surface charge density determination	265
Appendix D	Nonlinear regression analysis for transport mechanism of NaCl	267
<b>LIST OF PUBLICATIONS, SEMINARS AND AWARDS</b>		269



## LIST OF TABLES

Page

Table 1.1	Advantages of ceramic membranes (Lu <i>et al.</i> , 2007)	4
Table 1.2	Preparation methods of ceramic membranes (Lu <i>et al.</i> , 2007)	6
Table 1.3	Applications of ceramic membranes in liquid phase separations (Tsuru, 2003)	9
Table 2.1	Examples of previously reported works using various templates for pore templating in ceramics	31
Table 2.2	Bulk macroporous ceramics prepared using colloidal polymer sphere templates via various synthesis methods	32
Table 2.3	Summary of publications from 1990 based on fabrication of porous ceramics by sphere templating method (Hoa <i>et al.</i> , 2006)	36
Table 2.4	Bimodal porous ceramics with templated secondary pores	42
Table 2.5	Thin ceramic films with pores templated by spheres (Gulians <i>et al.</i> , 2004)	43
Table 2.6	Classification of pores recommended by IUPAC	44
Table 2.7	Examples of common ceramic membranes prepared by sol-gel process (Hsieh, 1996a)	45
Table 2.8	Examples of studies on $\gamma$ -alumina membrane for specific application	46
Table 2.9	Porous ceramic membranes in market (Hsieh, 1996a)	50
Table 2.10	Retention of salt by ceramic membranes reported since 1995	54
Table 2.11	Previous works reported on the separation of dye-salt-water mixture using NF membrane	60
Table 4.1	List of materials and chemicals used	80
Table 4.2	Full $3^2$ factorial DOE with 4 replicates for preliminary study on effect of organic compound and casting gap on tape thickness	83
Table 4.3	$2^2$ factorial DOE with 3 replicates for statistical evaluation on significance of tape thickness and organic content on permeability	87

Table 4.4	Full 3 <sup>2</sup> factorial DOE with 3 replicates for study on effect of tape thickness and organic content on support permeability	89
Table 4.5	Sample designation and the ratio of sol to template for each sample	92
Table 4.6	Designation of bi-layered membranes supported by $\alpha$ -alumina support	101
Table 4.7	Experimental conditions of dye-salt-water separation	109
Table 4.8	Experimental runs for dye-salt-water separation which were statistically chosen by Design Expert	110
Table 4.9	Constraints for optimum operation conditions of dye-salt-water separation using A025/Si	111
Table 5.1	Full 3 <sup>2</sup> factorial DOE with 4 replicates for preliminary study on effect of organic mixture and casting gap on tape thickness	113
Table 5.2	ANOVA result for response surface linear model for preliminary study on effect of organic mixture and casting gap on tape thickness	115
Table 5.3	2 <sup>2</sup> factorial DOE with 3 replicates for statistical evaluation on significance of tape thickness on permeability	120
Table 5.4	ANOVA result for 2 <sup>2</sup> factorial DOE for statistical evaluation on significance of tape thickness on permeability	122
Table 5.5	Full 3 <sup>2</sup> factorial DOE with 3 replicates for study on effect of organic content and tape thickness on support permeability	124
Table 5.6	ANOVA result for response surface reduced quadratic model for study on effect of organic content and tape thickness on support permeability	125
Table 5.7	ANOVA result for response surface reduced quadratic model for study on effect of organic content and tape thickness on support yield loss	126
Table 5.8	Characteristic of the mesoporous $\gamma$ -alumina samples after calcined at 500 °C for 1 hr	149
Table 5.9	Pseudo-first-order and pseudo-second-order rate constants of different types of porous material	150

Table 5.10	Calculated permeability coefficients, $k_\gamma$ and specific resistance, $r_m$ for $\gamma$ -alumina thin layers with different porosity supported on $\alpha$ -alumina supports	155
Table 5.11	Secondary porosity in bimodal porous $\gamma$ -alumina	158
Table 5.12	Overall permeability and thickness for silica/ $\gamma$ -alumina membranes supported on $\alpha$ -alumina supports	166
Table 5.13	Permeability and specific resistance of silica layers supported with different intermediate layers (A000, A025 and A050)	166
Table 5.14	Pore size and porosity of silica layers supported with different intermediate layers (A000, A025 and A050)	168
Table 5.15	Characteristics of the reactive dyes used	170
Table 5.16	Estimated osmotic pressure and predicted permeate flux	178
Table 5.17	Fitting observed permeate fluxes to kinetic model calculated from NaCl separation with different feed concentrations at pH 7	179
Table 5.18	Effective volume charge density $X_d$ for different bi-layered membranes	186
Table 5.19	Values of $F_l$ and $R_\infty$ for different bi-layered membranes calculated from NaCl separation with feed concentration of 5 mM	187
Table 5.20	Effect of membrane properties on diffusive and convective flow ( <a href="#">Ahmad and Ooi, 2006</a> )	188
Table 5.21	CCD arrangement and responses for NF of dye and salt mixture in aqueous solution	189
Table 5.22	Results of sequential model sum of squares and lack of fit test for dye rejection	192
Table 5.23	ANOVA result of response surface linear model for dye rejection	193
Table 5.24	ANOVA result of response surface reduced linear model for dye rejection	194
Table 5.25	Results of sequential model sum of squares and lack of fit test for salt rejection	199

Table 5.26	ANOVA result of response surface quadratic model for salt rejection	200
Table 5.27	ANOVA result of response surface reduced quadratic model for salt rejection	201
Table 5.28	Results of sequential model sum of squares and lack of fit test for permeate flux	208
Table 5.29	ANOVA result of response surface quadratic model for permeate flux	209
Table 5.30	ANOVA result of response surface reduced quadratic model for permeate flux	211
Table 5.31	ANOVA result of response surface final quadratic model for permeate flux	211
Table 5.32	Solutions for optimum operation conditions of dye-salt-water separation using A025/Si	219
Table B.1	Permeation data and calculated $R_{real}$ and concentration of NaCl at the wall for NaCl separation using A025/Si membrane	264

## LIST OF FIGURES

Page

Figure 1.1	Membrane markets in US\$ million ( <a href="#">Atkinson, 2005</a> ).	1
Figure 1.2	The filtration spectrum ( <a href="#">Koch Membrane Systems, 2004</a> ).	2
Figure 1.3	SEM micrograph of an asymmetric silica/ $\gamma$ -alumina membrane ( <a href="#">Samuel de Lint, 2006</a> ).	5
Figure 1.4	Preparation of ceramic membrane by the sol-gel method ( <a href="#">Burggraaf and Keizer, 1991</a> ).	7
Figure 2.1	Methods for assembling sphere array into colloidal crystal template. (Adopted from <a href="#">Velev and Lenhoff, 2000</a> )	37
Figure 3.1	Schematic concentration profiles layer.	66
Figure 4.1	Flow diagram of research.	79
Figure 4.2	Schematic diagram of the dead end filtration unit.	85
Figure 4.3	Schematic diagram of the experimental rig for liquid permeation test.	86
Figure 5.1	Predicted and observed values of tape thickness	116
Figure 5.2	(a) Contour plot and (b) surface response plot for preliminary study on the effect of organic mixture and casting gap on tape thickness.	118
Figure 5.3	Half-normal probability plot for support permeability as response.	121
Figure 5.4	Contour plots for effect of organic content and tape thickness on (a) support permeability and (b) support yield loss.	128
Figure 5.5	SEM picture of membrane support cross section which has been optimized with maximum permeability and minimum yield loss.	131
Figure 5.6	TEM pictures of nanosized PS beads.	132
Figure 5.7	PS bead size distribution prepared by emulsion polymerization.	133
Figure 5.8	TGA curves for A000, A025, A050 and A100	134
Figure 5.9	Viscosity of boehmite sol with different quantity of templating units added.	135
Figure 5.10	Newtonian model fit of viscosity for different sols.	136

Figure 5.11	TEM pictures of (a) A000, (b) A025, (c) A050 and (d) A100 after calcined at 500 °C for 1 hr.	138
Figure 5.12	FT-IR curves of (a) A000, (b) A025, (c) A050 and (d) A100 after calcined at 500 °C for 1 hr.	140
Figure 5.13	XRD patterns of (a) A000, (b) A025, (c) A050 and (d) A100 after calcined at 500 °C for 1 hr.	141
Figure 5.14	TEM pictures of A025 calcined at (a) 500 °C for 1 hr, (b) 500 °C for 3 hr, (c) 600 °C for 1 hr, (d) 600 °C for 3 hr, (e) 700 °C for 1 hr and (f) 700 °C for 3 hr.	143
Figure 5.15	TEM of A050 calcined at (a) 500 °C for 1 hr, (b) 500 °C for 3 hr, (c) 600 °C for 1 hr, (d) 600 °C for 3 hr, (e) 700 °C for 1 hr and (f) 700 °C for 3 hr.	144
Figure 5.16	N <sub>2</sub> adsorption and desorption isotherms for (a) A000, (b) A025 and (c) A050 after calcined at 500 °C for 1 hr.	146
Figure 5.17	Pore size distribution of $\gamma$ -alumina samples based on the BJH-model for the desorption branch of the nitrogen isotherms.	148
Figure 5.18	SEM pictures of (a) A000, (b) A025 and (c) A050 supported on $\alpha$ -alumina discs.	152
Figure 5.19	Product of water flux and viscosity vs. applied pressure of $\gamma$ -alumina thin layers with different porous structures supported on $\alpha$ -alumina support.	153
Figure 5.20	PEG retention curves of different $\gamma$ -alumina thin layers at 4 bar.	156
Figure 5.21	TEM picture of Si.	159
Figure 5.22	XRD pattern of Si with ordered nanopores after calcinations.	160
Figure 5.23	N <sub>2</sub> adsorption and desorption isotherms for silica after calcined at 450 °C for 45 min.	161
Figure 5.24	Pore size distribution of silica sample based on the BJH model for the desorption branch of the nitrogen isotherms.	161
Figure 5.25	The <i>t</i> -plot of surfactant templated silica after calcined at 450 °C for 45 min.	162

Figure 5.26	SEM and EDX images of the bi-layered membrane prepared with different intermediate layers (a) SEM image of A000/Si membrane, (b) SEM image of A025/Si membrane, (c) SEM image of A050/Si membrane, (d) the distribution of Si on A000/Si membrane by EDX (e) the distribution of Si on A025/Si membrane by EDX and (f) the distribution of Si on A050/Si membrane by EDX.	164
Figure 5.27	Product of water flux and viscosity vs. applied pressure of bi-layered membranes with different intermediate layers supported on $\alpha$ -alumina support.	165
Figure 5.28	PEG retention curves of different membranes at 4 bar.	167
Figure 5.29	Retention of RR120, RB5 and RO16 dyes solution with concentration of 1000 ppm at different pressure using (a) A000/Si (b) A025/Si and (c) A50/Si membranes.	171
Figure 5.30	Retention of RR120, RB5 and RO16 dyes solution with different concentrations at 10 bar using (a) A000/Si (b) A025/Si and (c) A050/Si membrane.	174
Figure 5.31	Permeate flux versus time for RB5 aqueous solution with feed concentration of 1000 ppm separated using (a) A000/Si, (b) A025/Si and (c) A050/Si at 4 bar and 10 bar.	176
Figure 5.32	Permeate flux versus time for RB5 aqueous solution with different feed concentrations separated using (a) A000/Si, (b) A025/Si and (c) A050/Si at 10 bar.	177
Figure 5.33	Salt retention of (a) A000/Si, (b) A025/Si and (c) A050/Si at different pressure for feed solutions with concentration of 5 mM and 10 mM.	181
Figure 5.34	Permeate flux of (a) A000/Si, (b) A025/Si and (c) A050/Si at different pressure for pure water (lines) and salt feed solutions with concentration of 5 mM (grey markers) and 10 mM (blank markers).	182
Figure 5.35	Mean retention of NaCl with concentration of 7.5 mM and various pH values at 10 bar using different membranes.	183

Figure 5.36	Permeation flux for NaCl separation at 10 bar with feed concentration at 7.5 mM using different membranes.	184
Figure 5.37	Predicted and observed values of dye rejection in percentage.	194
Figure 5.38	(a) Contour plot and (b) surface response plot for effect of pressure and feed concentration of dye on dye rejection.	196
Figure 5.39	Predicted and observed values of salt retention in percentage.	202
Figure 5.40	Perturbation plot for permeate flux.	203
Figure 5.41	(a) Contour plot and (b) surface response plot for effect of pressure and feed concentration of salt on salt rejection ( $C_{dye} = 2$ g/L).	206
Figure 5.42	(a) Contour plot and (b) surface response plot for effect of pressure and feed concentration of dye on salt rejection ( $C_{F, NaCl} = 50$ g/L).	207
Figure 5.43	Predicted and observed values of permeate flux.	212
Figure 5.44	Perturbation plot for permeate flux.	213
Figure 5.45	(a) Contour plot and (b) surface response plot for effect of pressure and temperature on permeate flux ( $C_{F, NaCl} = 50$ g/L, pH = 7, $C_{F, dye} = 2$ g/L).	215
Figure 5.46	(a) Contour plot and (b) surface response plot for effect of pressure and feed concentration of salt on permeate flux (temperature = 37.5 °C, pH = 7, $C_{F, dye} = 2$ g/L).	216
Figure 5.47	(a) Contour plot and (b) surface response plot for effect of pressure and on pH on permeate flux (temperature = 37.5 °C, $C_{F, NaCl} = 50$ g/L, $C_{F, dye} = 2$ g/L).	217
Figure A.1	Calibration curve of crystal ponceau 6R concentration and absorbance at 510 nm.	258
Figure A.2	Calibration curve of PEG concentration and absorbance at 535 nm for PEG 35000 and 20000.	258
Figure A.3	Calibration curve of PEG concentration and absorbance at 535 nm for PEG 10000 and 6000.	259
Figure A.4	Calibration curve of PEG concentration and absorbance at 535 nm for PEG 3000 and 1500.	259



Figure A.5	Calibration curve of PEG concentration and absorbance at 535 nm for PEG 600 and 400.	260
Figure A.6	Calibration curve of PEG concentration and absorbance at 535 nm for PEG 200.	260
Figure A.7	Calibration curve of dye concentration and absorbance at 530 nm for RR120.	261
Figure A.8	Calibration curve of dye concentration and absorbance at 592 nm (RB5) and 493 nm (RO16).	261
Figure A.9	Calibration curve of NaCl concentration and conductivity.	262
Figure A.10	Plot of $\log (q_e - q_t)$ vs. $t$ for samples A000, A050 and A100.	262
Figure A.11	Plot of $t/q_t$ vs. $t$ for samples A000, A050 and A100.	263

## LIST OF PLATES

**Page**

Plate 4.1	Membrane auto-casting machine for doctor blade casting.	82
Plate 4.2	Mixing flask with temperature controller for preparing boehmite sol.	91

## LIST OF SYMBOLS

$A$	Surface area of membrane ( $\text{m}^2$ )
$A_k$	Porosity of the membrane (dimensionless)
$A_{k1}$	Primary porosity (dimensionless)
$A_{k2}$	Secondary porosity (dimensionless)
$a_i$	Activity of ions (dimensionless)
$B$	Constant of kinetic model for permeate flux reduction ( $\text{L}\cdot\text{m}^{-2}\cdot\text{bar}^{-1}$ )
$b_i$	Convective coupling coefficient (dimensionless)
$C_0$	Initial dye concentration in solution (mg/L)
$C_{1,p}$	Permeation concentration of component 1 ( $\text{mol}/\text{m}^3$ )
$C_{2,p}$	Permeation concentration of component 2 ( $\text{mol}/\text{m}^3$ )
$C_b$	Concentration of bulk solution (mol/L)
$C_{i,f}$	Bulk feed concentration of component $i$ at the feed side ( $\text{mol}/\text{m}^3$ )
$C_{i,p}$	Permeate concentration of component $i$ ( $\text{mol}/\text{m}^3$ )
$C_{i,w}$	Concentration at the wall ( $\text{mol}/\text{m}^3$ )
$C_p$	Concentration of permeate (mol/L)
$C_t$	Dye concentration in solution at time $t$ (mg/L)
$c_i^m$	Concentration of component $i$ in the membrane ( $\text{mol}/\text{m}^3$ )
$D_{1,p}$	Hindered diffusivity of component 1 ( $\text{m}^2/\text{s}$ )
$D_{2,p}$	Hindered diffusivity of component 2 ( $\text{m}^2/\text{s}$ )
$D_{i,p}$	Hindered diffusivity ( $\text{m}^2/\text{s}$ )
$D_{i,\infty}$	Diffusion coefficient ( $\text{m}^2/\text{s}$ )
$F$	Faraday constant (96487 C/mol)
$F_1$	Indicator of diffusive transport (dimensionless)
$G$	Hydrodynamic lag coefficient (dimensionless)
$g$	Acceleration due to gravity ( $\text{m}/\text{s}^2$ )
$H$	Liquid film thickness (m)
$i$	Number of ions per molecule of solute (dimensionless)
$J$	Volumetric flux of permeate ( $\text{m}^3\cdot\text{m}^{-2}\cdot\text{s}^{-1}$ )
$J_1$	Permeate flux through primary pores ( $\text{m}^3\cdot\text{m}^{-2}\cdot\text{s}^{-1}$ )
$J_2$	Permeate flux through secondary pores ( $\text{m}^3\cdot\text{m}^{-2}\cdot\text{s}^{-1}$ )
$J_{ss}$	Steady-state flux ( $\text{L}\cdot\text{m}^{-2}\cdot\text{bar}^{-1}$ )

$J_t$	Permeate flux at time $t$ ( $\text{L}\cdot\text{m}^{-2}\cdot\text{bar}^{-1}$ )
$J_v$	Permeate volume flux based on membrane area (m/s)
$J_w$	Pure water permeate flux ( $\text{L}\cdot\text{m}^{-2}\cdot\text{hr}^{-1}$ )
$j_i$	Ion flux based on membrane pore area ( $\text{mol}\cdot\text{m}^2\cdot\text{s}^{-1}$ )
$j_v$	Volume flux based on membrane pore area ( $\text{m}^3\cdot\text{m}^{-2}\cdot\text{s}^{-1}$ )
$K$	Time constant of kinetic model for permeate flux reduction ( $\text{hr}^{-1}$ )
$K^{-1}$	Hydrodynamic enhanced drag coefficient (dimensionless)
$K^\circ$	Boltzmann's constant ( $1.38 \times 10^{-23}$ J/K)
$K_{i,c}$	Hindrance factor for convection (dimensionless)
$K_{i,d}$	Hindrance factor for diffusion (dimensionless)
$k$	Mass transfer coefficient (m/s)
$k_1$	Permeability coefficient of primary pores (m)
$k_2$	Permeability coefficient of secondary pores (m)
$k'$	Mass transfer coefficient by Equation 3.22 (dimensionless)
$k_f$	Rate constant of pseudo-first-order model (l/min)
$k_m$	Overall membrane permeability coefficients (m)
$k_s$	Rate constant of pseudo-second-order model ( $\text{mg}\cdot\text{g}^{-1}\cdot\text{min}^{-0.5}$ )
$k_\alpha$	Permeability coefficient of $\alpha$ -alumina support (m)
$k_\gamma$	Permeability coefficients of $\gamma$ -alumina layer (m)
$L_m$	Membrane thickness determined from SEM micrograph (m)
$L_p$	Solvent permeability of the membrane ( $\text{L}\cdot\text{m}^{-2}\cdot\text{bar}^{-1}$ )
$l$	Membrane thickness (m)
$MW$	Molecular weight of solute (Da)
$m$	Mass of unsupported $\gamma$ -alumina (g)
$n$	Number of data points in dye adsorption test (dimensionless)
$P$	Operating pressure (atm)
$q_e$	Adsorption capacity in equilibrium (mg/g)
$q_t$	Amount of dye adsorbed at time $t$ (mg/g)
$q_{t\text{ cal}}$	Calculated dye adsorbed value (mg/g)
$q_{t\text{ exp}}$	Experimental dye adsorbed value (mg/g)
$R$	Gas constant ( $8.314$ J.K <sup>-1</sup> .mol <sup>-1</sup> for Equation 3.2 and $0.08314$ L.bar.K <sup>-1</sup> .mol <sup>-1</sup> for Equation 4.18)
$R_{obs}$	Observed rejection of component $i$ (dimensionless)

$R_{real}$	Real rejection of component $i$ (dimensionless)
$R_{\infty}$	Indicator of convective transport (dimensionless)
$r$	Molecular radius of solute ( $\text{\AA}$ )
$r_i$	Stokes radius of component $i$ (m)
$r_m$	Specific resistance membrane ( $\text{m}^{-2}$ )
$r_p$	Pore radius (m)
$r_{p1}$	Primary pore radius (m)
$r_{p2}$	Secondary pore radius (m)
$r_r$	Radius of stirrer (m)
$T$	Temperature (K)
$U$	Withdrawal speed (m/s)
$V$	Volume of solution in <a href="#">Equation 4.3</a> (L)
$v_i$	Volume of solution in <a href="#">Equation 3.4</a> ( $\text{m}^3$ )
$X_d$	Effective membrane volume charge ( $\text{mol}/\text{m}^3$ )
$w_1$	Initial weight of permeate (g)
$w_2$	Final weight of permeate (g)
$z_i$	Valence of component $i$ (dimensionless)

#### Greek letters

$\Delta F$	Electrical potential difference (V)
$\Delta P$	Applied pressure drop (bar)
$\Delta q$	Normalized standard deviation (%)
$\Delta X$	Difference in potential (V)
$\Delta x$	Effective membrane thickness (m)
$\Delta \Psi_D$	Donnan potential difference at interface (V)
$\Phi_i$	Steric partition term (dimensionless)
$\Gamma$	Ratio of diffusive flow to convective flow (dimensionless)
$\gamma$	Shear rate ( $\text{s}^{-1}$ )
$\gamma_{LV}$	Liquid–vapor surface tension (N/m)
$\eta$	Viscosity (Pa.s)
$\mathcal{G}_i$	Molar mobility ( $\text{mol}.\text{m}^2.\text{J}^{-1}.\text{s}^{-1}$ )
$\lambda$	Ratio of solute to pore radius (dimensionless)

$\Delta\mu$	Chemical potential difference (V)
$\Pi$	Osmotic pressure (bar)
$\rho$	Density of permeate (g/cm <sup>3</sup> )
$\nu$	Kinematic viscosity (m <sup>2</sup> /s)
$\omega$	Stirring speed (s <sup>-1</sup> )
$\Psi$	Electric potential in axial direction (V)
$\psi$	Electrical potential (V)
$\rho$	Density (g/m <sup>3</sup> )
$\sigma$	Reflection coefficient (dimensionless)
$\tau$	Shear stress (D/cm <sup>2</sup> )

## LIST OF ABBREVIATIONS

BET	Brunauer–Emmett–Teller
BJH	Barrett-Joiner-Halenda
CCD	Central composite design
CF-ENP	Combined film theory-extended Nernst Planck equation
DOE	Design of experiments
DSPM	Donnan Steric Pore Model
EDX	Energy dispersive X-ray microanalysis
ENP	Extended Nernst-Planck model
FT-IR	Fourier-transform infrared
IEP	Isoelectric point
LLD	Landau–Levich–Derjaguin
MF	Microfiltration
MW	Molecular weight
MWCO	Molecular weight cut-off
NF	Nanofiltration
PEG	Polyethylene glycol
PMMA	Poly(methyl methacrylate)
PS	Polystyrene
PVA	Polyvinyl alcohol
RB5	Reactive Black 5
RO	Reverse osmosis
RO16	Reactive Orange 16
RR120	Reactive Red 120
RSM	Response surface method
SEM	Scanning electron microscope
TEM	Transmission electron microscope
TGA	Thermal gravimetric analysis
UF	Ultrafiltration
XRD	X-ray diffraction

# MEMBRAN SERAMIK BERLIANG DWIMOD MENGGUNAKAN PENCONTOH POLISTIRENA BERSAIZ NANO: SINTESIS, PENCIRIAN DAN PENILAIAN PRESTASI

## ABSTRAK

Membran seramik mempunyai rintangan yang tinggi terhadap haba dan bahan kimia, tetapi kebolehtelapannya adalah lebih rendah secara relatif berbanding dengan membran organik. Membran seramik dioptimumkan dalam kajian ini dengan memperkenalkan membran seramik berliang dwimod yang dipercontohkan dengan menggunakan sfera polistirena bersaiz nano. Lapisan  $\gamma$ -alumina berliang dwimod berjaya digunakan sebagai lapisan pertengahan untuk mengurangkan rintangan pengangkutan dalam membran silica/ $\gamma$ -alumina. Membran dwi-lapisan disokong atas penyokong  $\alpha$ -alumina yang disediakan daripada pita hijau. Pita hijau dihasilkan secara konsisten dengan menggunakan mesin penebaran automatik. Dalam reka bentuk eksperimen, kebolehtelapan penyokong  $\alpha$ -alumina didapati optimum pada  $30.86 \text{ L.m}^{-2}.\text{hr}^{-1}.\text{bar}^{-1}$  dengan mengurangkan ketebalan pita hijau dan memilih kandungan organik optimum.  $\gamma$ -Alumina berliang dwimod disediakan dengan menambahkan sfera polistirena (garis pusat  $\approx 50 \text{ nm}$ ) ke dalam sol boehmit. Selepas dikalsin pada  $500 \text{ }^\circ\text{C}$  untuk 1 jam, pencontoh disingkirkan dengan pengecutan liang yang kecil. Akan tetapi, liang sekunder teruntuh pada suhu yang lebih tinggi daripada  $500 \text{ }^\circ\text{C}$ . Kuantiti pencontoh kurang daripada  $0.5 \text{ g}$  dicadangkan untuk ditambahkan ke dalam  $20 \text{ ml}$  sol boehmit supaya dapat menghasilkan liang-liang sekunder tersusun. Dengan menggunakan kaedah pencirian penjerapan/penyaherapan  $\text{N}_2$ , sampel-sampel  $\gamma$ -alumina yang dioptimumkan menunjukkan garis pusat liang primer  $5 - 6 \text{ nm}$  dengan isipadu liang sekunder yang agak rendah. Berbanding dengan  $\gamma$ -



alumina berliang unimod,  $\gamma$ -alumina berliang dwimod yang tidak disokong menunjukkan kinetik resapan yang diperbaiki manakala lapisan  $\gamma$ -alumina berliang dwimod yang tersokong menunjukkan pengurangan rintangan spesifik sebanyak 48 %. Lapisan  $\gamma$ -alumina berliang dwimod banyak mengurangkan rintangan pengangkutan membran dwi-lapisan. Rintangan spesifik lapisan silika dikurangkan hampir 62 % apabila disokong atas lapisan  $\gamma$ -alumina berliang dwimod yang dioptimumkan. Dalam ujian pemisahan pewarna, penolakan pewarna bertambah dengan keberatan molekul pewarna manakala fluks penelapan berubah dengan masa. Fluks penelapan adalah lebih rendah daripada fluks air tulen; ini boleh dikaitkan kepada kombinasi pengutuban kepekatan dan penjerapan. Dalam ujian pemisahan garam, penolakan garam berkurang apabila komposisi garam suapan meningkat disebabkan kesan Donnan. Prestasi pemisahan adalah agak malar bagi membran berliang unimod: penahanan sistem dua lapisan dalam seluruh julat pH berubah di antara 60 % dan 70 %. Tambahan pula, penahanan NaCl berkurang dengan pertambahan isipadu liang sekunder. Model Nernst-Planck Lanjutan digunakan untuk mencirikan membran dwi-lapisan dengan struktur liang yang berlainan dalam istilah ketumpatan cas isipadu efektif ( $X_d$ ) dan mekanisme pengangkutan ion. Kaedah respons permukaan dengan rekabentuk komposit pusat dijalankan untuk mengkaji pengaruh keadaan operasi umum ke atas kualiti dan kuantiti telapan apabila membran silika/ $\gamma$ -alumina dengan lapisan pertengahan berliang dwimod yang dioptimumkan diaplikasikan dalam penapisan-nano campuran pewarna-garam-air. Penolakan perwarna yang dicapai melebihi 90 %. Model mencadangkan penahanan garam dipengaruhi oleh tekanan, kepekatan suapan pewarna dan garam. Akan tetapi, fluks telapan merosot disebabkan pengutuban kepekatan dan kekotoran.

# **BIMODAL POROUS CERAMIC MEMBRANE VIA NANOSIZED POLYSTYRENE TEMPLATING: SYNTHESIS, CHARACTERIZATION AND PERFORMANCE EVALUATION**

## **ABSTRACT**

Ceramic membranes possess great resistance toward heat and chemicals, but the permeability of ceramic membranes is relatively low compared to polymeric membranes. The ceramic membrane was optimized in this study by introducing bimodal porous ceramic membrane templated using nanosized polystyrene spheres. Bimodal porous  $\gamma$ -alumina layer was successfully utilized as intermediate layer in order to reduce transport resistance in silica/ $\gamma$ -alumina membrane. The bi-layered membrane was supported on  $\alpha$ -alumina support which was prepared from green tapes. The green tapes were uniformly fabricated using auto-casting machine. In the design of experiments, permeability of  $\alpha$ -alumina support was found to be optimum at  $30.86 \text{ L.m}^{-2}.\text{hr}^{-1}.\text{bar}^{-1}$  by reducing tape thickness and choosing optimum organic content. Bimodal porous  $\gamma$ -alumina was tailored by adding polystyrene spheres (diameter  $\approx 50 \text{ nm}$ ) into boehmite sol. After calcined at  $500 \text{ }^{\circ}\text{C}$  for 1 hr, template was removed with small pore shrinkage. However, secondary pores were demolished at higher temperature than  $500 \text{ }^{\circ}\text{C}$ . Template quantity less than 0.5 g was recommended to be added into 20 ml boehmite sol for creating ordered secondary pores. From the characterization results using  $\text{N}_2$  adsorption/desorption, the optimized  $\gamma$ -alumina samples showed primary pore diameter of 5 - 6 nm with relatively low secondary pore volume. Compared to unimodal porous  $\gamma$ -alumina, unsupported bimodal porous  $\gamma$ -alumina showed improved adsorption kinetic while supported bimodal porous  $\gamma$ -alumina layers showed more than 48 % reduction in the specific resistance. Bimodal

porous  $\gamma$ -alumina layer reduced the transport resistance of bi-layered ceramic membrane greatly. Specific resistance of silica layer reduced nearly 62 % when supported on the optimized bimodal porous  $\gamma$ -alumina layer. In dye separation test, the rejection of dye increased with molecular weight of dyes while the permeate flux varied with time. The permeate flux was lower than the corresponding pure water flux; which could be related to a combination of concentration polarization and adsorption. In the salt retention test, the salt rejection decreased when the feed salt composition increased due to the Donnan effect. The separation performance was relatively constant for unimodal porous membrane: the retention of the two-layer system over the whole pH range varied between 60 % - 70 %. Moreover, the retention of NaCl reduced with the increment of secondary pore volume. Extended Nernst-Planck model was used to characterize the bi-layered membrane with different porous structures in term of the effective volume charge density ( $X_d$ ) and the transport mechanism of ions. Response surface method with central composite design was performed to study the influence of common operating conditions on the quality and quantity of permeate when the optimized silica/ $\gamma$ -alumina membrane with bimodal porous intermediate layer was applied in the nanofiltration of dye-salt-water mixture. The rejection of dye achieved was more than 90 %. The model suggested that the salt retention was affected by pressure, the feed concentration of dye and salt. However, the separation was susceptible to flux decline due to concentration polarization and fouling.

# CHAPTER 1

## INTRODUCTION

### 1.1 Membrane Separation Technology

Advances in membrane separation technologies have been largely driven by the increasing environmental regulations enacted and the rising demand of desalinated water (Atkinson, 2005, Voutchkov, 2005). In comparison to conventional filters, distillation systems and ion exchange resins, membrane separation systems provide high quality products with acceptable energy consumption. An additional factor is the economic advantage of using membranes, as they reduce waste disposal expenditure and allow for increased opportunities for material recovery and recycling. Due to these reasons, the use of membrane in variety market places, such as water and wastewater treatment, as well as food and beverage processing is expanding significantly as shown in Fig. 1.1. In USA, the demand for membrane is forecasted to grow up to US\$ 2.9 billion in 2010 (Atkinson, 2005).

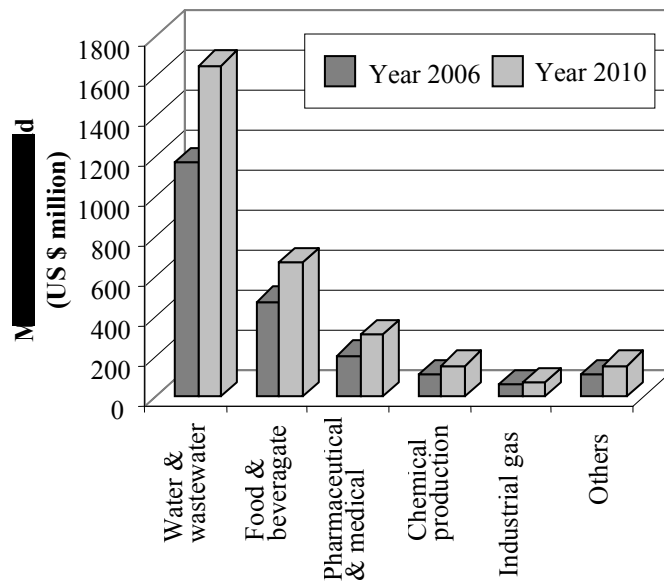


Fig. 1.1 Membrane markets in US\$ million (Atkinson, 2005).

There are four main types of membrane system commonly used in industry (Aptel and Buckley, 1996):

- (a) Microfiltration (MF) is widely applied in particulate removal process and maintains degreasing.
- (b) Ultrafiltration (UF) is generally used for oil, water and emulsion separations; paint recovery; and the separation of fats, oils or greases in the food industry.
- (c) Reverse osmosis (RO) and nanofiltration (NF) are used extensively for water purification, desalination and disinfection.

The classification of the membranes for MF, UF, NF and RO is illustrated in Fig. 1.2. The figure also shows the relative size of common retained materials, the membrane pore size and the approximated molecular weight cut-off (MWCO) of the membranes.

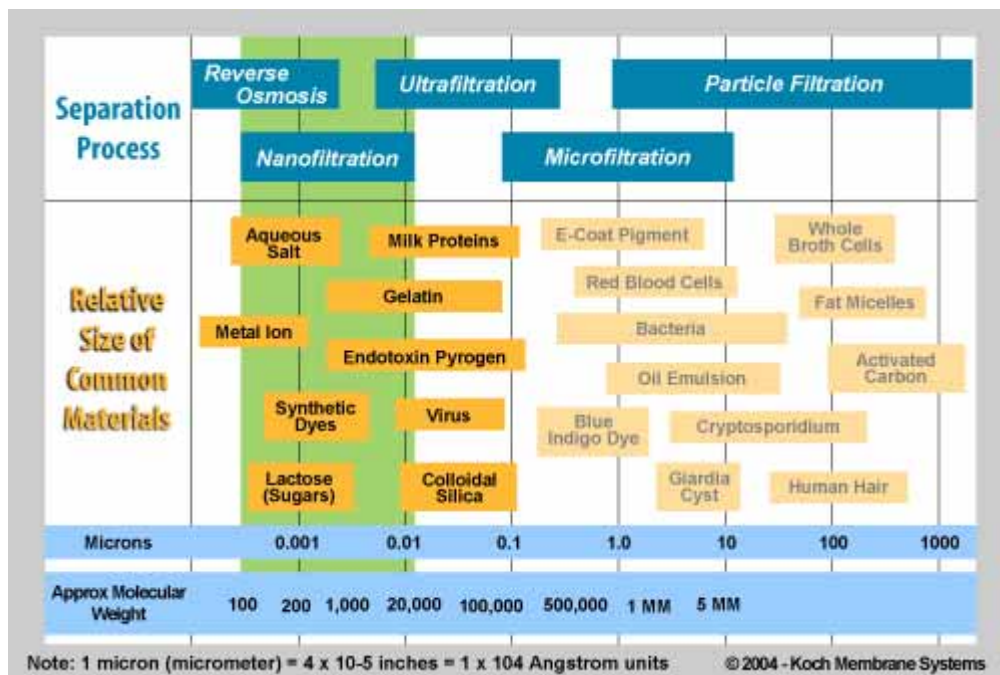


Fig. 1.2 The filtration spectrum (Koch Membrane Systems, 2004).

Using membrane separation correctly can provide financial savings and conserve resources. Maximum benefits are obtained when one or both the output streams from the membrane system are recycled or re-used, thereby reducing process materials requirement and minimizing waste disposal costs.

### **1.1.1 Nanofiltration (NF)**

NF is a pressure driven membrane separation process which is characterized by a membrane pore size ranging from 1 nm to 10 nm (Van Rijn, 2004). NF is categorized to be between conventional RO and UF as it can achieve high organic removal and moderate inorganic removals. Operating at moderate pressures (10 - 34 bar), NF membranes have high retention coefficients for neutral molecules with a molecular mass > 300 Da. NF membranes also have a surface electrostatic charge which gives them great selectivity with respect to ions or charged molecules (Henry *et al.*, 1997). Thus, NF is widely used in applications such as color removal, demineralization and desalination (Van Rijn, 2004).

Although NF membranes are able to separate ions from water, a high retention for multivalent ions is frequently combined with a moderate retention for monovalent ions. The removal of monovalent ions using NF membranes varies between 50 % to 90 % depending on the material and manufacture of the membrane (Oumar Anne *et al.*, 2001). Due to this reason, there are variety of NF membranes available, from physical solids (metal, ceramic, etc.), homogeneous films (polymer, metal, etc.) and heterogeneous solids (polymer mixes, mixed glasses, etc.). Polymeric membranes dominate the market because they are well developed and quite competitive in separation performance and economic (Atkinson, 2005).

However, inorganic membranes, including ceramic membranes, have been utilized to some extent in practical applications such as food, beverage and biotechnology (Hsieh, 1996b).

### 1.1.2 Ceramic membranes with high stability

Ceramic membranes are made of inorganic materials such as alumina, titania, zirconia oxides or some glassy materials (American Ceramic Society, 1920). Although ceramic membranes are considered to be costly due to the expensive starting materials, the complex fabrication process, and low membrane surface area per volume of a membrane module; ceramic membranes still have a lot of other advantages over polymeric membranes. Contrast to polymeric membranes, ceramic membranes possess benefits of thermal stability, resistance to solvent and chemical as listed in Table 1.1. Other advantages of ceramic membranes are high mechanical strength and long term durability (Bugraaf and Keizer, 1991, Hsieh, 1996b). However, it has to be noted that the advantages are dependent on the types of ceramics.

Table 1.1 Advantages of ceramic membranes (Lu *et al.*, 2007)

Advantages	Applications and comments
Thermal stability	<ul style="list-style-type: none"> <li>• Separation at high temperature, steam sterilization</li> </ul>
Resistance to organic solvents	<ul style="list-style-type: none"> <li>• Separation of non-aqueous systems, separation of oil</li> </ul>
Resistance to chemicals acidic and basic pH	<ul style="list-style-type: none"> <li>• Chemical cleaning, recovery of acid/base</li> </ul>
Resistance to peroxide	<ul style="list-style-type: none"> <li>• Chemical cleaning, application of textile processing</li> </ul>
Mechanical strength	<ul style="list-style-type: none"> <li>• Backwashing</li> </ul>
Long life-span	
Uniform pore size	<ul style="list-style-type: none"> <li>• Dependent upon preparation methods</li> </ul>

In general, ceramic membranes consist of thin ceramic layers supported on porous ceramic supports as shown in Fig. 1.3. Macroporous membrane supports which provide the major mechanical strength for pressure driven separation processes, are usually manufactured using oxide powders by extrusion or tape casting (Lindqvist and Liden, 1997, Terpstra *et al.*, 1998). The pore size of supports is usually larger than a micrometer and the support thickness is generally in order of few millimeters. An intermediate layer is coated on the support layer in order to reduce the pore size of coating surface for further coating of top layer. Meanwhile, the top layer which has the separation ability needs to possess controlled pore size which is suitable for the specific separation (Tsai *et al.*, 2000).

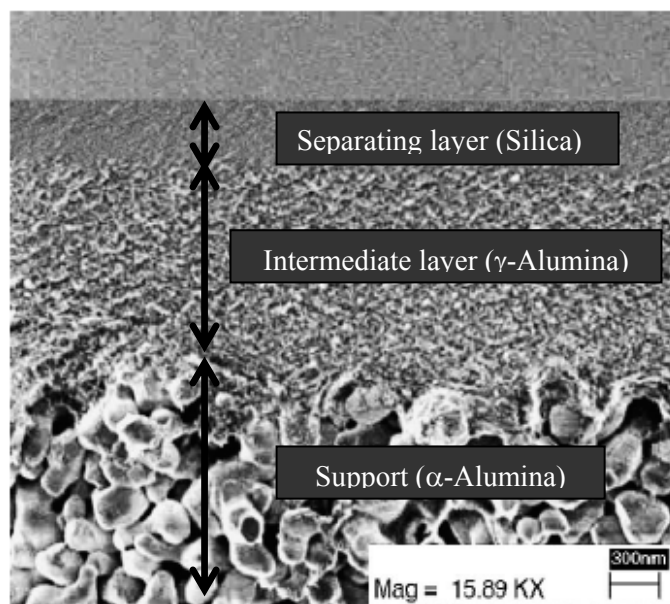


Fig. 1.3 SEM micrograph of an asymmetric silica/ $\gamma$ -alumina membrane (Samuel de Lint *et al.*, 2006).

In such structural design, the pore size of an asymmetric ceramic membrane shows a gradient structure from the porous supports to the separation layer, so as to minimize the resistance to permeation across the membrane. There are several methods to prepare intermediate layers and separating layers as listed in Table 1.2. The selection



of a preparation method depends on the desired membrane structure and the application of the membrane. For example, sol-gel route is prominent in preparing nanoporous ceramic membranes while chemical-vapor deposition is well-known in producing dense ceramic membranes (Lin, 2001).

Table 1.2 Preparation methods of ceramic membranes (Lu *et al.*, 2007)

Process	Materials
Sol-gel	$\gamma$ -Al <sub>2</sub> O <sub>3</sub> , SiO <sub>2</sub> , TiO <sub>2</sub> , ZrO <sub>2</sub>
Chemical vapor deposition	SiO <sub>2</sub>
Pyrolysis	SiC, Si <sub>3</sub> N <sub>4</sub>
Hydrothermal treatment	Silicalite
Anodic oxidation	Al <sub>2</sub> O <sub>3</sub> (Amorphous)
Phase separation/ leaching	SiO <sub>2</sub>
Dynamic membranes	ZrO <sub>2</sub> (Amorphous)

### 1.1.3 Sol-gel method for the preparation of ceramic membranes

Sol-gel method is the most common approach of creating ceramic thin films. The high and keen interest in sol-gel synthesized materials is contributed by a number of apparent reasons. Highly porous materials and nanocrystalline materials can be created with controlled pore size, porosity and desired pore wall chemistry. In addition, liquid precursors are used so it is possible to cast ceramic membrane into desired modules without involvement of extremely high temperature. Addition of organic species may serve as templates for creation of pores with preferred size and shape as well (Wright and Sommerdijk, 2001).

Sol-gel methods are classified into two categories, colloidal sol method and polymeric sol method depending on formation route of the sol (Anderson *et al.*,

1988, Burggraaf and Keizer, 1991, Larbot *et al.*, 1988). The processes are shown schematically in Fig 1.4. In the colloidal sol route, a metal alkoxide dissolved in alcohol is hydrolyzed by addition of excess water or acid. The resulted precipitate is maintained as a hot solution for an extended period in order to form a stable colloidal solution. The colloidal solution is then cooled and coated onto the membrane support. The liquid film ought to be carefully dried to avoid defects such as cracks and pinholes. The metal oxide films are formed after sintering at 500 - 800 °C.

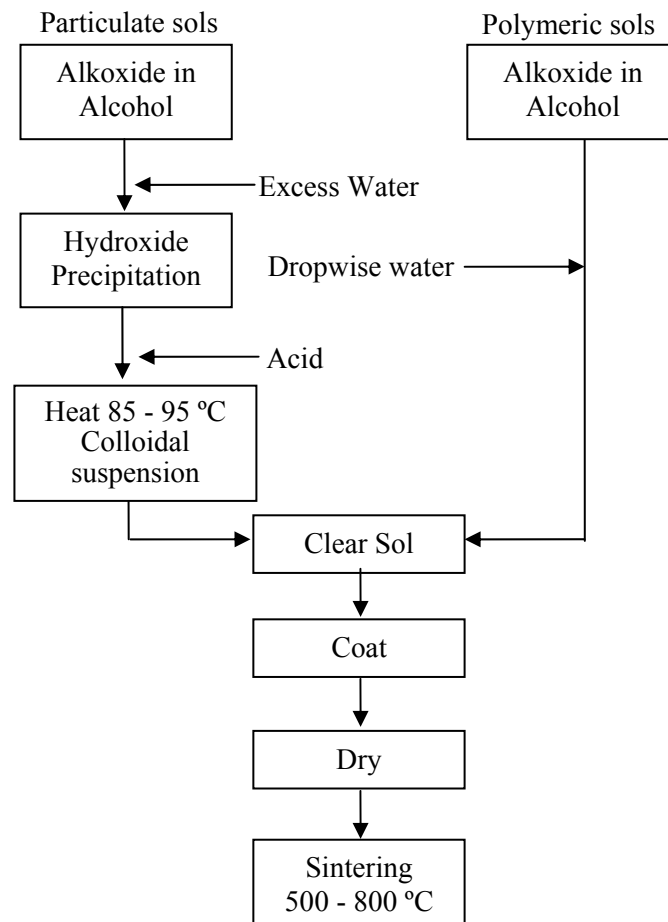
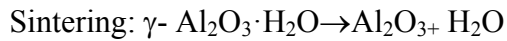
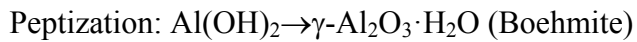
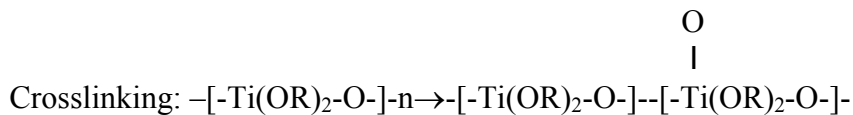
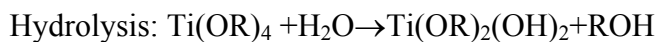


Fig. 1.4 Preparation of ceramic membrane by the sol-gel method (Burggraaf and Keizer, 1991).

For instance, the overall process for the preparation of  $\gamma$ -alumina membrane using colloidal route can be represented as (Baker, 2000):



In the polymeric sol-gel process, partial hydrolysis of a metal alkoxide dissolved in alcohol is accomplished by adding the minimum of water to the solution. The active hydroxyl groups on the alkoxides react to form an inorganic polymer molecule which can be coated on membrane supports. On drying and sintering, the metal oxide film forms. Chemically the polymeric sol-gel process for titania membrane can be represented as follows (Baker, 2000):



The pore size of sol-gel derived membranes is most influenced by the size of the sols in both methods. For the case of the colloidal sol route, pore size is controlled by the void spaces among the packed colloidal particles. Meanwhile, the size of the gel network determines the membrane pore size when the polymeric gel is used. Compared to colloidal sol, the polymeric sol is more suitable to form microporous membranes since the size of the gel network is smaller than the size of colloidal sols. In general, the pore size of sol-gel derived membranes can be controlled in the range of 0.5 – 50 nm depending on the sol properties and other

factors such as addition of binder and heat treatment (Lambert and Gonzalez, 1999). For creation of hierarchical porous structure, secondary pores can be generated by adding template in the sol and removing template in the solidification step (Hoa *et al.*, 2006). In this case, primary pores are void spaces among the packed colloidal particles or gel networks while the secondary pores are templated using additional templating units.

#### 1.1.4 General application of ceramic membranes in liquid phase separation

Ceramic membranes have been extensively applied in areas such as food and beverage industry; biotechnology and pharmaceutical industry; chemical and industrial applications; recovery and recycling as summarized in Table 1.3. The ability of ceramic membranes to uniquely address the distinct needs of frequent cleaning, high resistance of harsh operating conditions and continuous flow in these areas is the main reason why ceramic membranes are preferred choice over other types of membranes (Finley, 2005).

Table 1.3 Applications of ceramic membranes in liquid phase separations (Tsuru, 2003)

Area	Process	Application examples
Food and beverage industry	MF and UF	<ul style="list-style-type: none"> <li>Concentration of milk, concentration of protein, clarification of fruit juice, clarification of wine, bacteria removal, microorganism separation from fermented.</li> </ul>
Biotechnology and pharmaceutical industry	MF and UF	<ul style="list-style-type: none"> <li>Microorganism separation and cell debris filtration, plasma separation.</li> </ul>
Chemical and industrial applications	MF and UF	<ul style="list-style-type: none"> <li>Oil-water separation, purification of used oil, removal of precipitated heavy metals and solids.</li> </ul>
Recovery and recycling	UF and NF	<ul style="list-style-type: none"> <li>Drinking water and wastewater treatment.</li> </ul>

MF and UF ceramic membranes have been used in a wide variety of filtration processes such as separation of microorganism, proteins and colloidal solutes (Cheryan, 1998, Sondhi *et al.*, 2003). NF on the other hand, has the largest applications in water treatment, including wastewater containing heavy metals and synthetic dyes (Bougen *et al.*, 2001, Duke *et al.*, 2007, Voigt *et al.*, 2001b). For wastewater treatment, nanoporous ceramic membranes with charged surface not only retain electrolytes under steric effects but also Donnan effects (Combe *et al.*, 1997). Ion separation is primarily due to the electrostatic interaction between ions and surface charge. The co-ions with the same charge as the membrane surface, create repulsive force from the membrane surface which is termed as Donnan exclusion. Hence, ion separation can be successfully carried out using NF membranes even though the ions are much smaller than membrane pores (Rios *et al.*, 1996, Tsuru *et al.*, 1998a).

In addition, the application of ceramic membranes has also been extended to non-aqueous solution separation especially in petrochemical processing where organic membranes cannot be utilized. Alumina, silica and zirconia UF membranes have been applied to the separation of asphaltene from crude oil in the temperature range of 155 – 180 °C (Guizard *et al.*, 1993). The treated oils are reported to be considered as clean oils owing to the effective removal of heavy metals such as copper, lead, chromium and iron (Higgins *et al.*, 1993). The permeation properties through porous membranes are determined by the affinity between feed solutions with the membrane surface. Unlike UF and MF, the mechanism through inorganic porous membranes in the NF range is an activated process and does not obey the viscous flow mechanism (Tsuru, 2003). Another interesting application is the use of

ceramic membranes for separation and concentration of organic solvent such as ethanol and hexane (Tsuru *et al.*, 2001b, Wu and Lee, 1999). Silica and silica–zirconia membranes, prepared by a sol–gel process, have been successfully utilized in separating non-aqueous solvent mixtures (Asaeda *et al.*, 1998, Tsuru *et al.*, 2001b). Furthermore, ceramic membranes can be applied in supercritical fluids separation especially supercritical CO<sub>2</sub> (Sarrade *et al.*, 1996) and supercritical alcohol (Brasseur-Tilmant *et al.*, 2000).

Although ceramic membranes can be applied in various applications, NF using ceramic membranes is not widely practiced compared to organic membranes. It is due to few problem statements which are further discussed in the next section.

## **1.2 Problem Statements**

The preparation of sol-gel derived ceramic membranes is of tremendous importance since the utilization of ceramic membranes can be extended beyond separation and purification such as membrane reactor. Despite all the advantages as mentioned in Section 1.4, sol-gel method is not without limitations. Particular ageing, drying and sintering are required for a desired porous structure. Although membrane pores can be tailored precisely by incorporating solid template, this method is rarely adopted for the preparation of membrane. Besides that, proper calcination for template removal is important to prevent pore shrinkage or even pore collapse. Such details of sol-gel method with additional template definitely need a full understanding in order to exploit the advantages of templating method in membrane preparation where it cannot be attained by other methods.

Even though ceramic membranes possess high resistance against heat and chemicals, the permeability to liquid and gases is relatively low compared to organic membranes. The attempt to reduce the membrane thickness is always restricted by the occurrence of defects. Therefore, the ceramic membrane performance has to be optimized in such a way that the permeability improvement does not impair the other advantage features of membranes. In this study, the templated pores occur as secondary pores which have been proven to enhance adsorption. It is certainly a necessity to investigate the possibility of permeability increment by introducing secondary pores into ceramic membrane since it has not been studied widely elsewhere.

In order to form ceramic thin layers through sol-gel method, consistent and reproducible supports are required. The membrane supports also have to introduce minimum resistance to permeation and persist well in the pressure driven separation. The membrane supports are prepared by sintering the pelletized green tapes which offers fine surface for coating. Thus, this study has to include design of experiments to study the effects of green tape characteristics on the support permeability.

Before preparation of thin ceramic layers with templated pores, it is also important to decide the suitable quantity of templating units and calcination conditions in order to avoid defects such as disorder pore arrangement, pore shrinkage and pore collapse. For certain ceramics such as  $\gamma$ -alumina, solid templating method usually results in serious pore shrinkage and collapse of pore wall after calcinations. Although  $\gamma$ -alumina is often the most favorable porous ceramics in catalysis and membrane technology owing to the high pore volume, large surface

area and great catalytic properties, not much related work has been reported in the past about the preparation of bimodal porous  $\gamma$ -alumina. Due to these reasons, a preliminary study with the purpose of tailoring secondary pores precisely in  $\gamma$ -alumina is definitely a must in this research.

In this research, bimodal porous  $\gamma$ -alumina is employed as intermediate layer in silica/ $\gamma$ -alumina membrane to improve membrane permeability. In order to gauge the effectiveness of the newly developed membranes, phenomenological properties of bi-layered membranes such as pure water permeability and MWCO are essential. These properties need to be determined for bi-layered ceramic membranes to understand the effects of secondary pore volume in the intermediate layer. However, having this information alone is not sufficient as they are not related to the mechanistic structure of a membrane. As a result, the membrane performance is structurally impractical to be optimized. Thus, the research has to focus on the membrane structural properties such as pore size, effective thickness/porosity and effective volume charge density which are evaluated from the membrane separation performance in the retention test of uncharged solutes and charged solutes.

Once the effects of secondary pore volume on the structural properties and the separation performance is fully understood, the optimized membrane needs to be properly tested in the separation of dye-salt-mixture. This is because optimized ceramic membrane possesses great potential to be applied in textile wastewater containing water soluble reactive dye which is difficult to be removed using conventional method. Besides that, the treatment process usually involves hot effluent and frequent cleaning. It is highly important to study and gather some initial



information on the separation performance of nanoporous ceramic membranes which is most suitable for textile wastewater treatment. The information is crucial for further improvement of membrane application especially in module selection and separation design in the future.

### **1.3 Research Objectives**

The present research has the following objectives:

1. To synthesize nanoporous ceramic membrane with ordered pores using templating method.
2. To increase permeability of sol-gel derived ceramic membrane by introducing secondary pores.
3. To develop ceramic supports with improved permeability by controlling green tape characteristics for supporting membrane efficiently.
4. To develop nanoporous ceramic with bimodal pore size distribution and enhanced diffusive transportation through sol-gel method with addition of templates.
5. To study the effect of secondary pores in intermediate layer on separating layer formation and membrane properties such as pore size, effective thickness/porosity and effective charge density.
6. To investigate the performance of bi-layered membrane with different secondary pore volume in the separation of organic ions (dyes) and inorganic ions (salt).
7. To study optimal operating conditions for improved bi-layered membrane in separating dye-salt-water system.

#### 1.4 Research Scope

The present research includes the preparation of  $\alpha$ -alumina supports with improved permeability. The membrane supports are prepared by sintering the pressed alumina green tapes. In order to form supports with high permeability, influences of tape characteristics such as thickness (0.025 - 0.035 mm) and organic content (10.61 - 14.24 %) are studied.

The technique to produce the supported  $\gamma$ -alumina thin layer with ordered secondary pores using nanosized polystyrene (PS) beads is disclosed. Before being engineered into thin layer, the effect of template quantity (0 - 0.05 g/ml sol) on sol characteristics is investigated. The template quantity chosen is to make sure the formation of defect free thin layer of  $\gamma$ -alumina with ordered secondary pores. The thermogravimetric behavior and the sol viscosity are the sol characteristics changes which are interesting to be studied. The calcined unsupported oxides with different secondary pore volumes are characterized using transmission electron microscope (TEM), Fourier-transform infrared (FT-IR) and X-ray diffraction (XRD). The heat treatment effect on the templated porosity is also investigated. Under appropriate calcination treatment, the optimized templated  $\gamma$ -alumina is prepared for porosity and adsorption kinetic study.

The supported  $\gamma$ -alumina thin layers with different pore volumes are further studied using scanning electron microscope (SEM) for thickness comparison. Besides determining the membrane permeability using dead end stirred cell, individual layer permeability and specific resistance of bimodal porous membrane is calculated. Polyethylene glycol (PEG) retention test is carried out to determine basic

characteristics of supported  $\gamma$ -alumina layers such as MWCO, pore size and ratio of effective thickness to porosity.

The research is continued with the coating of surfactant templated silica sol on supported  $\gamma$ -alumina thin layers. The main objective is to improve the permeability of silica/ $\gamma$ -alumina membrane by utilizing bimodal porous intermediate layer. The effect of secondary pore volume on the separating layer characteristics is explored in this study. The possible structure and permeability changes of silica layer are not only analyzed using energy dispersive X-ray microanalysis (EDX) but also studied through water permeation test and PEG retention test.

Membrane is generally high in permeability but low in rejection or vice versa. Organic ions and inorganic ions are employed to test the separation performance of improved bi-layered membranes regarding the steric effect and Donnan effect in separation. The selected organic ions are reactive dyes with various molecular weights (617.54 Da, 991.80 Da and 1469.98 Da ([Sigma-Aldrich, 2007](#))) which are higher than the MWCO of silica/ $\gamma$ -alumina membranes. Process variables such as pressure (4 – 10 bar), dye concentration (0.25 - 1.00 g/L) and type of dyes (Reactive Orange 16 (RO16), Reactive Black 5 (RB5) and Reactive Red 120 (RR120)) are studied. On the other hand, NaCl is the chosen inorganic salt where the ion hydrated size (for  $\text{Na}^+ = 0.42$  nm and  $\text{Cl}^- = 0.39$  nm) is smaller than the membrane pore size. The variables such as pressure (6 – 10 bar), salt concentration (5 mM and 10 mM) and pH (pH 4 - 10) are studied. Besides that, the effective surface charge volumes of bi-layered membranes with different pore volume are determined by fitting salt separation results to Donnan Steric Pore Model (DSPM). The effective charge

volume is the membrane charge along the surface and through the pores which is responsible for Donnan effect. The salt separation results are also further analyzed using Extended Nernst-Planck Model (ENP) for studying the changes of salt transport mechanism.

In the last part of this research, separation of dye-salt-water mixtures is carried out using the bi-layered membrane with improved permeability. Response surface method (RSM) with central composite design (CCD) is performed to study influences of common operating conditions on the quality and quantity of permeate. The CCD is composed of five factors: temperature (25 – 50 °C), feed concentration of dye (1 - 3 g/L), feed concentration of salt (20 – 80 g/L), pH (pH 5 - 9) and pressure (5 - 10 bar). The responses which are of interest in this study are the percentage retention of dye, the percentage retention of salt, and the permeate flux. Polynomial models are used to represent the significant effects of the operational conditions on the interested responses. It is important to determine optimum conditions for achieving high rejection of dye and permeate flux. However, the worst salt rejection has to be predicted at the same time for designing the subsequent desalting step. The information helps in bimodal porous membrane application especially in module selection and separation design.

## **1.5 Organization of the Thesis**

The thesis consists of six chapters as listed in Table of Contents. A brief introduction on membrane separation technology with emphasis on NF is given in Chapter 1 (Introduction). The introduction of ceramic membranes and their preparation method as well as their general application in liquid phase are also

included in this chapter. The first chapter also includes the problem statements in order to provide some basis and rationale to identify the research directions to be followed in this study. On the basis of problem statement defined, the specific objectives of the research are then elaborated in detail together with the research scope. The organization of thesis is given in the last section of this chapter.

Chapter 2 (Literature Review) provides essential information of ceramic membranes. The preparation methods of ceramic support especially tape casting are analyzed in the beginning of the chapter. Sphere templating method in preparing porous ceramics is then chronologically discussed in the subsequent section. The third section of the chapter includes the development of sol-gel derived ceramic membranes. The application of ceramic membranes in the separation of neutral solutes and charged solutes is also discussed. In the last part of literature review, special emphasis on dye-salt-water is included.

The summary of the transport model used in this study is available in Chapter 3 (Nanofiltration Transport Model). First part of the chapter includes transport equations in the ENP. DSPM is then discussed in detail including equilibrium partitioning and concentration polarization. Combined Film Theory- extended Nernst Planck Equation (CF-ENP) is explained briefly in the last part of the chapter.

Chapter 4 (Materials and Method) presents the detail of materials and chemicals used in the present study. This is followed by the detailed experimental procedures, which include the membrane preparation method, characterization methods and analytical techniques. The synthesis method for both membrane support

and sol-gel derived membrane are discussed in detail, which include the preparation of template. The characterization method for membrane physicochemical properties such as thermogravimetric behavior, types of interatomic bonds, crystalline phase and porous structure are also outlined in Chapter 4. Details of the experimental set-up are then elaborated in this chapter. The procedure to carry out the permeation test in dead-end filtration unit is explained in detail. The permeation test includes water, PEG in aqueous solution, dye solutions, salt solutions and dye-salt-water mixtures for determination of membrane pore size, effective thickness/porosity, effective volume charge density and morphology.

Chapter 5 (Results and Discussion) is the core of this thesis, which presents, discusses and explains of the five main studies as listed in Table of Contents. In the first section, the effects of green tape characteristics on the supports permeability is studied to produce suitable supports with reduced resistance. The characteristics of unsupported ceramic with bimodal pore size distribution are explored in the second section. After selecting appropriate template quantity and heat treatment conditions, the supported  $\gamma$ -alumina thin layers with different pore volumes are further studied in the third section. The bimodal porous  $\gamma$ -alumina is utilized in bi-layered membrane for permeability improvement. The fourth study mainly focuses on the effects of secondary pore volume on the separating layer characteristics and separation performance in dye and salt solutions. DSPM and ENP model are used to study the effects of secondary pore on separation performance of the membrane. The last study includes the finding of optimum conditions for the improved membrane in separation of dye-salt-water mixtures.

The study's findings are recapitulated in Chapter 6 (Conclusions and Recommendations). The primary findings in Chapter 5 which include the effects of secondary pores on membrane formation, membrane characteristics and separation performance are summarized and concluded in this chapter. Based on the findings, recommendations for future research are suggested. Finally, closing remarks are stated in the last section of this chapter.

## CHAPTER 2

### LITERATURE REVIEW

#### 2.1 Membrane Supports for Sol-gel Derived Membranes

Ceramic supports are available commercially in various geometries such as disc, tube, multi-channel tube and honeycomb monolith. In general, alumina is the dominant material used for ceramic supports due to its high stability and inert feature (Grangeon and Lescoche, 1998). A proper ceramic support for sol-gel derived membrane must possess high permeability, great mechanical strength, fine finishing, large porosity and defined pore size (Luyten *et al.*, 2000). The pore size distribution of supports varied largely from 0.1  $\mu\text{m}$  to 15  $\mu\text{m}$ . Supports with average pore diameters larger than 1  $\mu\text{m}$  are considered as macroparticle filters (Morgart *et al.*, 1993). Recent publication on support layer preparation is relatively lean in the open literature even though synthesis methods of micro to nano-filter ceramic layers are reported extensively. This is possibly because traditional shaping processes are well adopted in most cases for the preparation of ceramic membrane support.

##### 2.1.1 Common preparation methods of membrane supports

The most common shaping processes used in traditional ceramic products are dry pressing, extrusion and tape casting. The choice of traditional ceramic processing method for preparing membrane supports is selected based on the desired geometry and microstructure of the ultimate products. Different processing techniques give different effects on the microstructural development of ceramic supports during sintering and will lead to different characteristics (Ribeiro *et al.*, 2004). Most methods begin with the preparation of ceramic formulations which involves wet



dispersion of ceramic powder in solvent with 30 – 70 wt % of solid loading and some additives such as binder. After milling the mixture, it is usually followed by shaping, dehydration and sintering (Ribeiro *et al.*, 2004).

Macroporous ceramic supports with symmetric structure are mainly produced by dry pressing and extruding methods. Dry compaction of ceramics for the synthesis of such supports has been reported by a few researchers (Chao and Chou, 1996, Chou *et al.*, 1998, Falamaki *et al.*, 2004, Liang *et al.*, 2006). They have investigated the effects of the ceramic particle size, binder quantity, pressing pressure and sintering temperature on support microstructure, i.e. porosity, pore size distribution and tortuosity. The support properties in terms of permeability and flexural strength were also measured and found to be related to both processing and microstructure parameters. In further comparison with other processing methods such as extrusion and slip casting, it was learnt that different degrees of homogeneity and particle packing achieved in the green state affect the final microstructures and material properties (Maarten Biesheuvel and Verweij, 1999, Ribeiro *et al.*, 2004). Compared to dry pressed supports, extruded ceramic supports not only possess better homogeneity and particle packing but they also offer the preferable tubular geometry which can be integrated in the cross flow separation systems. Besides tubular geometry, extrusion method can even be used to synthesize multi-channel tubular membrane supports (Ismagilov, 1997) and ceramic hollow fibers with larger surface area per unit packing volume (Vercauteren *et al.*, 1998). Recently, Isobe and co-workers (2007a, 2007b) have successfully increased the permeability of ceramic supports by tailoring uni-directionally oriented pores using plastic substance as a pore former via extrusion. Although macroporous supports prepared by dry pressing

and extrusion are low in cost, inhomogeneous packing results in ceramic products with lower tensile strength and poor surface smoothness (Maarten Biesheuvel and Verweij, 1999). The macroporous support is usually further dip coated or slip coated for producing asymmetric structure which is more applicable for sol coating of membrane (Luyten *et al.*, 2000).

Since additional modification step is needed, the mentioned traditional ceramics processing methods are time and cost consuming. Preparation of asymmetric ceramic supports in a single step has been the subject of interest. Centrifugal casting was reported in preparing tubular ceramics with gradient pore size (Biesheuvel *et al.*, 1998, Fukui, 1990). Nevertheless, this preparation method is not widely described in the literature because of its limitation in mass production. Tape casting, a conventional ceramics processing method in electronic industry is more suitable in producing asymmetric membrane supports over centrifugal casting as discussed below.

### **2.1.2 Tape casting of asymmetric membrane supports**

Tape casting is well established for the production of multilayer capacitors, insulating substrates and packages in electronic industry. This technique has been adopted in membrane technology to produce membrane supports typically ceramic substrates in flat configuration with thickness in order of few millimeters (Hsieh, 1996a). The preparation of ceramic supports using tape casting method has been well disclosed in the open literature. The greatest advantage of tape casting supports is the fine finished surface for sol coating without defects. Stacking tapes with increasing pore former quantity creates asymmetric porous structure which features largely in

porous structure of tape casting supports. The asymmetric structure is preferable as transport resistance is lower, especially in liquid filtration.

Tape casting methodology starts with the formulation stage where slurries are prepared by dispersing ceramic powder in solvent. Studies showed that ceramic powder with smaller particle size is preferable for high quality of finishing surface and smaller pore size (Das and Maiti, 1999); however, higher concentration of additives is required to prevent serious tape shrinkage (Pagnoux *et al.*, 1998). Since the last decade, non-aqueous slurries containing organic solvents such as alcohols, ketones and hydrocarbons have been replaced gradually by aqueous based slurries in most tape casting processes due to environmental and health concern. Although physical properties of green tapes from both types of slurries are similar, the aqueous system is more sensitive to process perturbations (Nahass *et al.*, 1990). A tape casting slurry must be adjusted in order to yield green tapes with satisfactory flexibility, cohesion, homogeneity and mechanical strength after sintering. This requires careful selection of the slurry additives together with accurate control of processing parameters. The ceramics powder and additives (i.e. dispersant, binder, plasticizer) should be added in a proper sequence to produce homogenous slurry with minimum agglomerates (Nahass *et al.*, 1990). The slurry preparation step frequently starts with a milling procedure in which ceramic powder is mixed with a solvent containing dispersant. Then a mixing and homogenization step occurs in which binders and plasticizers are added to the low viscosity slurry.

Since well-dispersed slurry is a prerequisite in the preparation of homogeneous and dense tape using tape casting method, dispersant which is also